

## Improving the quality of thermoplastic composite corners using laser-assisted tape placement

Daniël Peeters<sup>1</sup>, David Jones<sup>1</sup>, Ronan O'Higgins<sup>1</sup>, Paul M. Weaver<sup>1</sup>

<sup>1</sup> University of Limerick, School of Engineering, Bernal Institute, daniel.peeters@ul.ie

**Keywords:** thermoplastic composite, laser-assisted tape placement, manufacturing, out-of-autoclave

### Abstract

Over the past 25 years, interest in using thermoplastic composites in commercial and military aircraft has steadily increased. Combining winding and laser-assisted tape placement is a promising method to manufacture thermoplastic structures out-of-autoclave, as has been recently shown by manufacturing a variable stiffness, unitized, integrated-stiffener thermoplastic wingbox at the University of Limerick. The corner regions are one of the critical points of the structure and need to be characterized in more detail, for example by unfolding L-shaped samples in a 4-point bend test. In this work, samples with both 10mm and 3mm radii have been manufactured and tested. Two manufacturing parameters are varied: the speed and acceleration around the corners. The tests show that decreasing the radius has a positive influence on the corner strength. In addition, the highest speed and acceleration investigated lead to the highest corner strength for the same radius.

### 1 Introduction

Over the past 25 years, interest in using thermoplastic composites (TPC) in commercial and military aircraft has steadily increased. Starting with their first applications with the US military's F-22 fighter jet landing-gear and weapons-bay doors in the 1980s [1], applications now include the fixed wing leading edge on the Airbus A380 [2]. TPCs are of interest due to their potential for fast forming and weldability, their inherently superior fatigue performance and their excellent fire/smoke/toxicity (FST) properties compared with thermoset composites. Furthermore, the potential of these materials to manufacture large thermoplastic aerospace structures in a cost effective manner by out-of-autoclave (OOA) processing is appealing.

Recently, an OOA, variable stiffness, unitized, integrated-stiffener thermoplastic wingbox demonstrator was built and successfully tested at the University of Limerick [3]. An advantage of a unitized structure is the reduced number of separate parts and lower ensuing assembly costs, in contrast to a conventionally constructed wingbox which uses angle sections to connect skins to webs. This means that, contrary to traditional metallic structures, no L-brackets are reinforcing the corners. Hence, all the section forces have to be transmitted through the corners by the composite material. Furthermore, stress analysis of the wingbox shows that the highest stress concentrations are in the corners, as shown in Figure 1.

Both the wingbox and the stiffeners were made using winding in combination with laser-assisted tape placement (LATP). Detailed characterisation of coupon specimens from the wingbox was limited, as only one demonstrator was produced. The stiffeners were characterized in more detail: the bond strength between skin and stiffener was found to be satisfactory (46MPa) [4], but the tests for the corners were inconclusive [5]. A typical outcome of the 4-point bend test on an L-shaped specimen can be seen in Figure 2. The test was inconclusive because the test standard could not be adhered to: the stiffener was too small. The reason for the failure could either be the 3-dimensional stress introduced into the tested

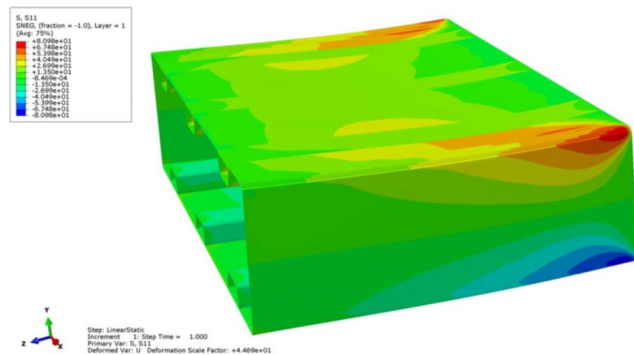


Figure 1.  $\sigma_{11}$  for the wingbox.

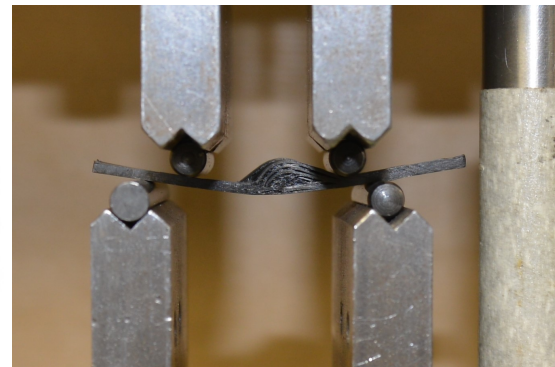


Figure 2. Example of 4-point bend test outcome.

part because of the close roller spacing, the radius being too small, or the un-optimised manufacturing parameters, for example lay-down speed and acceleration. In this study, L-shaped test samples with dimensions that respect the guidelines of the test standard have been manufactured to assess the ability to produce corners with good mechanical properties using winding in combination with LATP.

When using thermoset material to produce L-shaped samples, it is challenging to obtain angles of exactly 90° due to spring-in during cooling [6]. Wrinkling can also be a problem, arising from the length difference between the inside and the outside of a corner [7]. Surprisingly, wrinkles were shown to have a positive effect on the amount of spring-in: due to the lower stiffness, the amount of spring-in was reduced. Experimentally, the number of wrinkles that occurred was increased by bending the complete stack rather than every single ply while laying down [8].

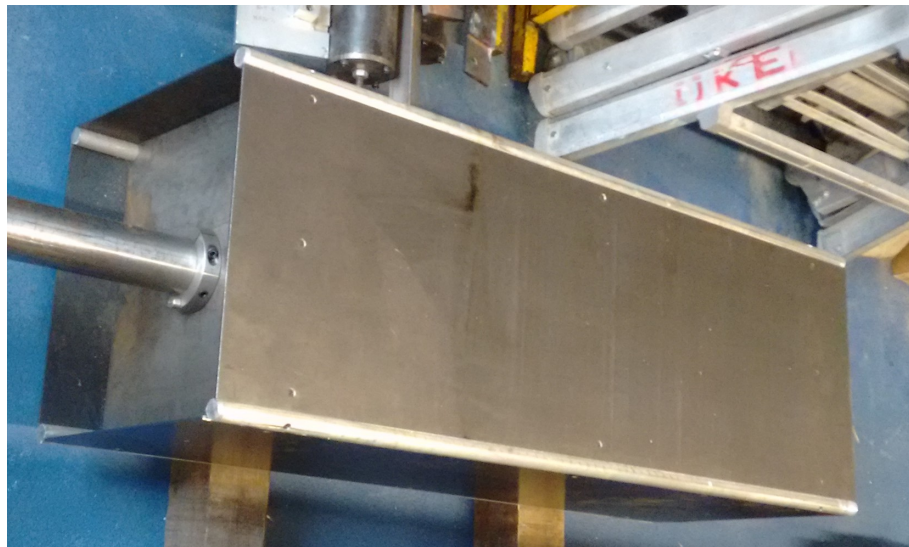
Other manufacturing techniques that can be used to obtain L-shaped samples include pultrusion, braiding, or compression moulding. When using pultrusion, the fibres are pulled through into a certain shape. Different cross-sections can be obtained, but the spring-in angle is dependent on the distance from the die exit [9, 10]. A combination of braiding and pultrusion can be used as well, but the achievable lay-ups are restricted: no uni-directional part can be achieved. The resulting structure is found to be well consolidated [11]. A more general overview can be found in Ismet et al. [10]

To check the strength of corners, in the current work samples with the correct dimensions were produced by manufacturing a box and cutting it into L-shaped test samples, as discussed in section 2. Next the test method and initial results are discussed in section 3. A comparison with previously published results and detailed discussion of the results are provided in section 4. The paper concludes with section 5.

## 2 Manufacturing

L-section test specimens were harvested from LATP wound square box-sections. Two different tools were used: one with a radius of 10mm, another with a radius of 3mm. These geometries allow the influence of the radius of the tool to be assessed, as well as different manufacturing parameters, in this case the rotational speed and acceleration.

The 10mm-tool consists of steel sides with the corners made out of solid aluminium bars. This system presents a challenge to remove the parts off the tool without breakage. The tool has been designed to be collapsible by removing the aluminium bars, which should give sufficient leeway to remove the box from the mould. A photograph of the mould can be seen in Figure 3(a). The 3mm-tool has been designed with a different principle: 4 separate box-sections with rounded edges are kept together with an end-connector. To allow some movement, a 2mm aluminium shim is placed between the blocks which can be removed after manufacturing, allowing the sections to collapse and be removed without damaging the composite box section. A photograph of the mould can be seen in Figure 3(b).



(a) Tool with a 10mm radius.



(b) Tool with a 3mm radius.

**Figure 3. Tools used during manufacture.**

The manufacturing parameters to be varied are the speed and acceleration around the corners. Since the work follows on from that done for the wingbox and stiffeners [3], the same linear speed over the straight parts is used:  $3m/min$ . This is relatively slow, and would need increasing for industrial use. During rotation the head of the robot has to accurately move over a significant distance which limits the maximum attainable speed. The speed and acceleration of the rotation for the stiffeners were  $200^\circ/sec$  and  $1000^\circ/sec^2$  respectively.

To assess the effect of processing parameters on the corner properties, box sample coupons were processed with varying rotational speed, rotational acceleration and thickness according to Table 1. Box 1 is used to assess whether thinner specimens can be used, while box 2 and 5 are made according to the same manufacturing parameters as the stiffeners [5]. L-section test specimens were cut from the box coupons and sanded down to a smooth finish. No delaminations were observed in the finished samples. All sample dimensions satisfied the standard requirements [12] as shown in Figure 5.

In Table 1, thickness 1 denotes the thickness in the leg before the corner, thickness 2 is the thickness in the corner, and thickness 3 denotes the thickness in the leg after the corner, as shown in Figure 4. The first observation is that the thickness of box 1 shows a different trend compared to other boxes: the corner is thicker in box 1, while it is thinner in the other boxes. However, this difference is relatively small and could be due to the tolerance in the measurements. Another noticeable point is that the change in thickness is larger in box 2 than in box 3 and 4. Finally, the increased thickness of box 5 and 6 compared to the other boxes stands out: the shorter edges on this tool seem to have an influence.

**Table 1. Overview of the manufacturing parameters and thicknesses.**

box number [—]	rotational speed [°/sec]	rotational acceleration [°/sec <sup>2</sup> ]	radius [mm]	average thickness 1 (std. dev.) [mm]	average thickness 2 (std. dev.) [mm]	average thickness 3 (std. dev.) [mm]
1	200	1000	10	1.070 (0.031)	1.087 (0.013)	1.075 (0.030)
2	200	1000	10	2.378 (0.053)	2.202 (0.032)	2.332 (0.063)
3	150	750	10	2.216 (0.038)	2.189 (0.039)	2.237 (0.054)
4	200	750	10	2.152 (0.042)	2.106 (0.024)	2.132 (0.054)
5	200	1000	3	2.439 (0.032)	2.421 (0.031)	2.439 (0.042)
6	150	750	3	2.366 (0.044)	2.380 (0.034)	2.391 (0.035)

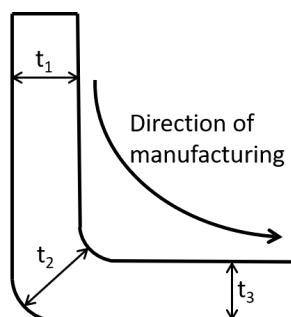


**Figure 4. Numbering of the points at which the thickness is measured.**

### 3 Tests

Corner strength was assessed by a 4-point bending testing carried out according to ASTM Standard D6415 [12], as shown in Figure 5(a). The specimens are almost exactly as the test standard suggests: 25mm wide, legs that are of appropriate length, an angle of 90°, and a thickness that is 2.2mm for boxes 2 to 6. Box 1 is only 1.1mm thick. The radius of the corner is not the prescribed 6.4mm in the test standard, but was chosen to be either 10mm or 3mm.

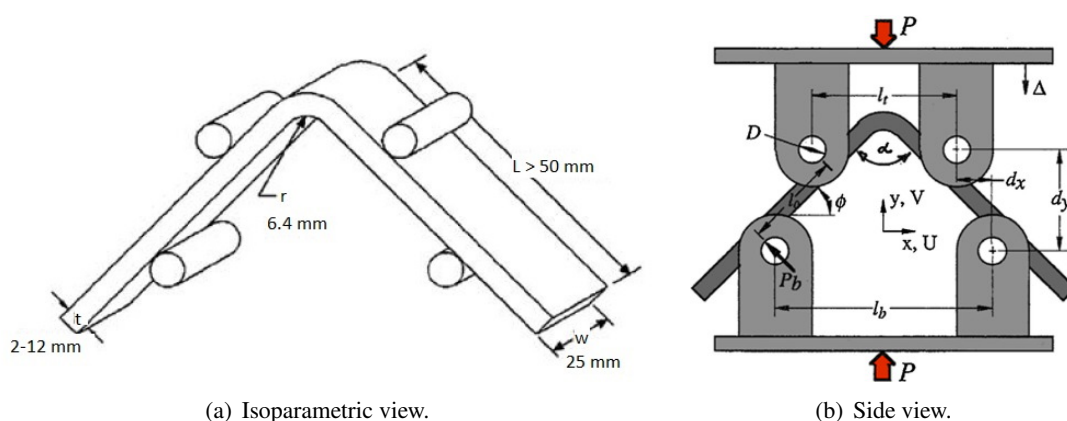


**Figure 5. Schematic view of the 4-point bend test according to ASTM D 6415.**

The goal of this test is determining the curved beam strength (CBS) which is calculated using [12]

$$CBS = \frac{M}{w} = \left( \frac{F}{2 \cdot w \cdot \cos(\phi)} \right) \cdot \left( \frac{d_x}{\cos(\phi)} + (D+t) \cdot \tan(\phi) \right) \quad (1)$$

where  $M$  denotes the moment,  $w$  the width of the specimen,  $F$  the total force,  $\phi$  the angle,  $D$  is the diameter of the cylindrical loading bars,  $t$  is the thickness of the sample and  $d_x$  denotes the distance in x-direction between the upper and lower bar. These dimensions are shown schematically in Figure 5(b). The angle  $\phi$  changes during the test, and can at any moment be calculated using

$$\phi = \text{Arcsin} \left( \frac{-d_x \cdot (D+t) + d_y \cdot \sqrt{d_x^2 + d_y^2 - D^2 - 2 \cdot D \cdot t}}{d_x^2 + d_y^2} \right) \quad (2)$$

where  $d_y$  denotes the distance in y-direction between the inner and outer roller, calculated using

$$d_y = d_x \cdot \tan(\phi_0) + \frac{D+t}{\cos(\phi_0)} - \Delta \quad (3)$$

where the subscript 0 denotes the initial angle (i.e., at the start of the test), and  $\Delta$  denotes the displacement in y-direction of the rollers.

From the CBS, the radial stress in a curved beam segment can be calculated using the method originally proposed by Lekhnitskii [13]. This has the advantage that the result is no longer dependent on the thickness of the sample, and results can be readily compared to each other. The stress in radial direction can be calculated using [13]

$$\sigma_r = -\frac{CBS}{r_o^2 \cdot g} \cdot \left( 1 - \frac{1 - \rho^{\kappa+1}}{1 - \rho^{2\kappa}} \left( \frac{r_m}{r_o} \right)^{\kappa-1} - \frac{1 - \rho^{\kappa-1}}{1 - \rho^{2\kappa}} \rho^{\kappa+1} \left( \frac{r_o}{r_m} \right)^{\kappa+1} \right) \quad (4)$$

where  $r_o$  denotes the outer radius of the test specimen. The other terms are defined as

$$g = \frac{1 - \rho^2}{2} - \frac{\kappa}{\kappa+1} \cdot \frac{(1 - \rho^{\kappa+1})^2}{1 - \rho^{2\kappa}} + \frac{\kappa \rho^2}{\kappa-1} \cdot \frac{(1 - \rho^{\kappa+1})^2}{1 - \rho^{2\kappa}} \quad (5)$$

$$\kappa = \sqrt{\frac{E_\theta}{E_r}} \quad (6)$$

$$\rho = \frac{r_i}{r_o} \quad (7)$$

$$r_m = \left( \frac{(1 - \rho^{\kappa-1}) \cdot (\kappa+1) \cdot (\rho r_o)^{\kappa+1}}{(1 - \rho^{\kappa-1}) (\kappa-1) r_o^{-(\kappa-1)}} \right)^{\frac{1}{2\kappa}} \quad (8)$$

where  $E_\theta$  is the  $E_{11}$  modulus and  $E_r$  can be assumed to be equal to  $E_{22}$ . For the material used,  $E_{11} = 135\text{GPa}$  and  $E_{22} = 7.54\text{GPa}$ .

During the test of the samples of box 1 to 4 it was observed that delaminations usually occurred in an adjacent straight region before the corner, rather than after the corner as was observed during the testing of the stiffener. The onset of delamination occurred rapidly: a cracking sound was heard during the test followed by a significant reduction in load. This suggests that a good bond was achieved for all the samples.

The average radial stress at maximum load and standard deviation for each of the four boxes is shown in Table 2. For box 2 and 3 only 4 samples were tested due to manufacturing and testing issues respectively. For box 1 and 4, the testing was performed on 8 samples. The standard deviations observed are relatively small for box 1, 2, and 4, only for box 3 the tests show considerable scatter. More test samples will need to be done to determine the significance and cause of such scatter.

Observing the results, it is noted that the benchmark (box 2) gives the highest radial stress. Even though the same manufacturing parameters were used for box 1, the radial stress is clearly lower. However, this

sample was half the thickness recommended by the standard and the failure mechanism is different to the other specimens, as was also indicated by Thurnherr et al. [14]. Slowing down the acceleration and speed during the rotation does not lead to a higher corner strength, on the contrary: the maximum radial stress is reduced by 8% when only the acceleration is reduced to  $750^\circ/sec^2$ , and by 12% when both the speed is reduced to  $150^\circ/sec$  and acceleration to  $750^\circ/sec^2$ .

Test specimens with a 3mm radius did not exhibit the same trend as observed for the 10mm radius specimens: the test samples delaminated in the region between the rollers rather than in the corner. Hence, the results are a lower limit of the radial stress, not the ultimate that can be achieved. This is why the results are highlighted in Table 2. The delamination is most likely due to use of the smaller tool: since the edges are shorter the head is constantly accelerating and decelerating. The higher thickness measured for box 5 and 6 also indicates a poor bond is present. Another indication for poor bond strength is the lower interlaminar shear strength (ILSS) found when testing specimens harvested from a stiffener with short sides [5] compared to the ILSS obtained from samples using a larger plate [4]. Only three samples were tested for each case since the failure mode was different from that expected.

**Table 2. Overview of the radial stress found.**

box number [—]	rotational speed [°/sec]	rotational acceleration [°/sec <sup>2</sup> ]	radius [mm]	average radial stress [MPa]	standard deviation radial stress [MPa]
1	200	1000	10	30.78	2.60
2	200	1000	10	37.04	2.71
3	150	750	10	32.66	4.35
4	200	750	10	33.97	2.54
5	200	1000	3	47.16	7.14
6	150	750	3	47.98	5.10

#### 4 Discussion

Since the radial stress is often found to be independent of the thickness [15, 16], this is used to compare the current results to previous ones in literature. Only one paper was found where a clear difference in radial stress for samples with different thickness was measured [17], however no specific reason is given for this. It is difficult to directly compare the results since no results for the same material, or any other CFRP thermoplastic with continuous fibres for that matter, were found. Using a thermoplastic matrix and short carbon fibres [18], a maximum radial stress of 21MPa was measured for a thickness of 2mm and a radius of 3 or 5mm. For a larger radius, the maximum radial stress decreased to 12MPa.

When considering thermoset materials, the maximal radial stress obtained is usually in the range of 27 to 36MPa [15, 19, 16]. A value of 36 – 40MPa was measured for a range of thicknesses (4, 8, and 12mm), and a radius equal to the thickness, independent of the lay-up [15]. Another study found that for 3 and 6mm thick specimens with a radius being either 3 or 6mm, the maximum radial stress was around 30MPa [16]. While Redman et al. [19] identified 27 – 28MPa as maximum radial stress for a 3mm thick specimen. The only study that finds a significantly lower radial stress was done for thick laminates: 20, 40 and 60 plies, with a radius to thickness ratio of 0.8, 1 and 1.5 [17]. The maximal radial stress was 7 – 8MPa for the thinnest material and only 4 – 5MPa for the thickest laminate. However, this difference could be, at least in part, due to the increasing radius.

Comparing the current results for box 1 to 4 to these, the maximum stress is found to be comparable to previously published results. The results found for box 2 are even higher than most results, indicating the promise thermoplastic materials have. Furthermore, it should be emphasised that even after delaminations developed, the force only dropped by around 40%. This load-carrying capability after delamination

is another significant advantage of using thermoplastic materials compared to thermoset materials. For box 5 and 6 an even higher corner stress is found, which is in line with the trend of a decreasing radius leading to an increase in maximum corner stress.

Even though the results for the 3mm tool are not fully conclusive, these preliminary results are already sufficient to conclude that the low corner strength found for the stiffener was not due to the manufacturing parameters or the corner radius. Hence, it is most likely that the small size of the samples tested from the stiffener is the main reason for the low corner strength found.

## 5 Conclusion

The combination of winding and laser-assisted tape placement is a promising method to manufacture thermoplastic structures in an out-of-autoclave process. Corner strength is a critical design parameter that requires characterization: contrary to traditional manufacturing methods, no L-shaped stiffening elements are present in the corners meaning all the stress is transferred through the composite material. Previously reported results [5] show that the corner strength could be relatively low, but the specimens that were used deviated from the test standard [12] in dimensions, stacking sequence and corner radius.

In the current work, specimens were manufactured and tested according to ASTM Standard D6415 [12]. The speed and acceleration in the corner were varied to determine their influence on the corner strength. Two different corner radii were checked: 3mm and 10mm. The tests for the 10mm radius showed that the higher speed and acceleration lead to a higher corner strength. An increase in thickness also lead to a higher corner strength. Even though the test for the 3mm radius did not give an upper limit for the corner strength, the minimum corner strength was significantly higher than the one found for the 10mm radius. This result indicates that the corner strength for small radii is even better than for larger radii.

Future work includes manufacturing samples that will be able to give the corner strength for smaller corner radii to confirm these initial findings. Furthermore, the linear speed should also be increased to investigate the potential to speed up the current manufacturing technology to industrial scale.

## Acknowledgements

The authors would like to thank Science Foundation Ireland (SFI) for funding Spatially and Temporally VARIABLE COMPOSITE Structures (VARICOMP) Grant No. (15/RP/2773) under its Research Professor programme. The authors would also like to thank ICOMP for its help with the LATP.

## References

- [1] "F-22A Raptor Advanced Tactical Fighter," <http://www.airforce-technology.com/projects/f22/>, Accessed: 23 February 2018.
- [2] Pora, J., *Composite Materials in the Airbus A380 - From History to Future*, 2001, Beijing, China.
- [3] Oliveri, V., Peeters, D., Clancy, G., O'Higgins, R., Jones, D., and Weaver, P. M., "Design, optimization and manufacturing of a unitized thermoplastic wing-box structure," *2018 AIAA/ASCE/AHS/ASC Structures, Structural Dynamics, and Materials Conference*, 2018.
- [4] Bandaru, A. K., Clancy, G., Peeters, D., O'Higgins, R., and Weaver, P. M., "Interface Characterization of Thermoplastic Skin-Stiffener Composite Manufactured Using Laser-assisted Tape Placement," *2018 AIAA/ASCE/AHS/ASC Structures, Structural Dynamics, and Materials Conference*, 2018.
- [5] Peeters, D., Clancy, G. J., Oliveri, V., O'Higgins, R., Jones, D., and Weaver, P. M., "Thermoplastic Composite Stiffener Design with Manufacturing Considerations," *2018 AIAA/ASCE/AHS/ASC*

*Structures, Structural Dynamics, and Materials Conference*, 2018, p. 0479.

- [6] Barnes, J., Byerly, G., LeBouton, M., and Zahlan, N., “Dimensional stability effects in thermoplastic composites towards a predictive capability,” *Composites Manufacturing*, Vol. 2, No. 3, 1991, pp. 171 – 178, *Flow Processes in Composite Materials '91*.
- [7] Potter, K., Khan, B., Wisnom, M., Bell, T., and Stevens, J., “Variability, fibre waviness and misalignment in the determination of the properties of composite materials and structures,” *Composites Part A: Applied Science and Manufacturing*, Vol. 39, No. 9, 2008, pp. 1343 – 1354.
- [8] Çinar, K. and Ersoy, N., “Effect of fibre wrinkling to the spring-in behaviour of L-shaped composite materials,” *Composites Part A: Applied Science and Manufacturing*, Vol. 69, 2015, pp. 105 – 114.
- [9] O’Connor, J., “Method for making variable cross section pultruded thermoplastic composite articles,” Oct. 1 1989, US Patent 5,026,447.
- [10] Baran, I., Cinar, K., Ersoy, N., Akkerman, R., and Hattel, J. H., “A Review on the Mechanical Modeling of Composite Manufacturing Processes,” *Archives of Computational Methods in Engineering*, Vol. 24, No. 2, Apr 2017, pp. 365–395.
- [11] Lebel, L. L. and Nakai, A., “Design and manufacturing of an L-shaped thermoplastic composite beam by braid-trusion,” *Composites Part A: Applied Science and Manufacturing*, Vol. 43, No. 10, 2012, pp. 1717 – 1729, *CompTest* 2011.
- [12] ASTM Standard D6415, “standard test method for measuring the curved beam strength of a fiber-reinforced polymer-matrix composite,” *ASTM International*, 2002.
- [13] Lekhnitskii, S. G., “Anisotropic plates,” Tech. rep., Foreign Technology Div Wright-Patterson Afb Oh, 1968.
- [14] Thurnherr, C., Groh, R., Ermanni, P., and Weaver, P., “Investigation of failure initiation in curved composite laminates using a higher-order beam model,” *Composite Structures*, Vol. 168, 2017, pp. 143 – 152.
- [15] Charrier, J.-S., Laurin, F., Carrere, N., and Mahdi, S., “Determination of the out-of-plane tensile strength using four-point bending tests on laminated L-angle specimens with different stacking sequences and total thicknesses,” *Composites Part A: Applied Science and Manufacturing*, Vol. 81, No. Supplement C, 2016, pp. 243 – 253.
- [16] Avalon, S. C. and Donaldson, S. L., “Strength of composite angle brackets with multiple geometries and nanofiber-enhanced resins,” *Journal of Composite Materials*, Vol. 45, No. 9, 2011, pp. 1017–1030.
- [17] Hao, W., Ge, D., Ma, Y., Yao, X., and Shi, Y., “Experimental investigation on deformation and strength of carbon/epoxy laminated curved beams,” *Polymer Testing*, Vol. 31, No. 4, 2012, pp. 520 – 526.
- [18] Wan, Y., Goto, T., Matsuo, T., Takahashi, J., and Ohsawa, I., *Investigation about fracture mode and strength in curved section of carbon fiber reinforced polypropylene*, 2013, Montreal, Canada.
- [19] Arca, M. A. and Coker, D., “Experimental investigation of CNT effect on curved beam strength and interlaminar fracture toughness of CFRP laminates,” *Journal of Physics: Conference Series*, Vol. 524, No. 1, 2014, pp. 012038.